An analysis of the first steps of phenol adsorption-oxidation over coprecipitated Mn–Ce catalysts: a DRIFTS study

Oriana D'alessandro, Horacio J. Thomas & Jorge E. Sambeth

Reaction Kinetics, Mechanisms and Catalysis

ISSN 1878-5190
Volume 107
Number 2

Reac Kinet Mech Cat (2012) 107:295-309
DOI 10.1007/s11144-012-0470-0

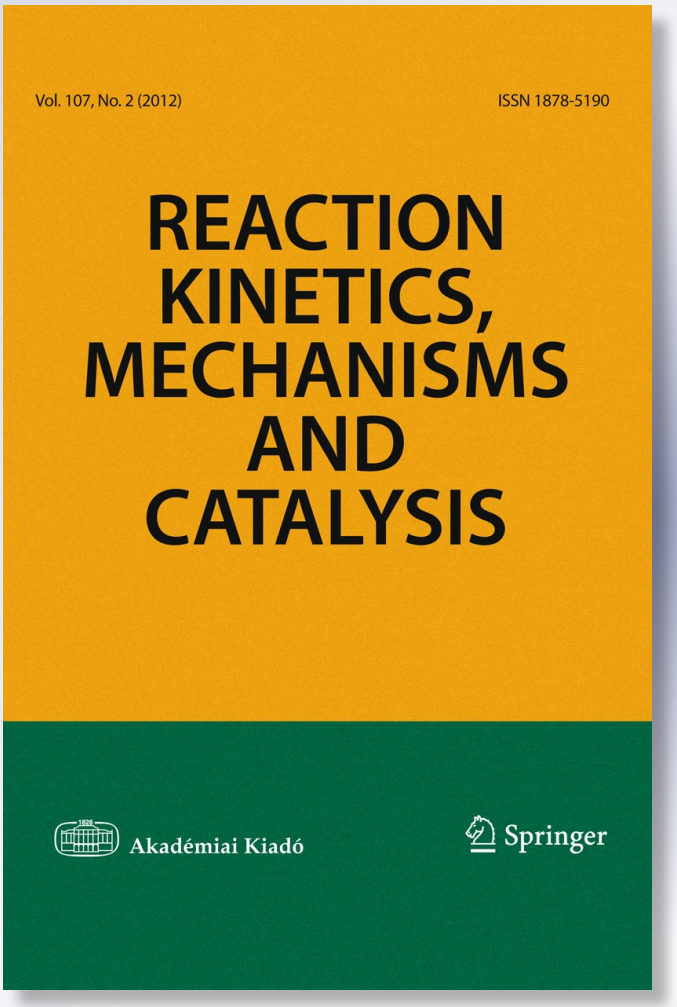

Springer

Reac Kinet Mech Cat (2012) 107:295–309
DOI 10.1007/s11144-012-0470-0

An analysis of the first steps of phenol adsorption-oxidation over coprecipitated Mn–Ce catalysts: a DRIFTS study

Oriana D'alessandro · Horacio J. Thomas · Jorge E. Sambeth

Received: 25 February 2012 / Accepted: 2 June 2012 / Published online: 23 June 2012

Abstract A series of Mn–Ce(M) solids (M = K or Na), with molar ratios 100–0, 50–50 and 0–100 were prepared by co-precipitation of manganese and cerium nitrate from NaOH or KOH solutions at pH = 11. In addition, part of the solids precipitated with NaOH were dried and impregnated with a Cu^{2+} salt. The solids were characterized by XRD, Specific Surface Area, XPS and EDS. The characterization analyses show the formation of Mn mixed oxides with different oxidation states (Mn^{3+}, Mn^{4+}), for samples without Ce or Mn–Ce(M) 50–50. In the latter solid and in the one where there is no Mn, the formation of CeO_2 (fluorite type) was detected. The samples were tested in the phenol removal in water at 100 °C and at atmospheric pressure with the aim to analyze the adsorbed species in the first stage of the adsorption-oxidation mechanisms. The results indicate, on the one hand, that [MnO_x] is the active species in the process and that the most active solids are those that present (i) a higher concentration of O_I, (ii) a higher amount of Mn^{4+} ions. DRIFT spectroscopy showed a possible mechanism of phenol adsorption on two sites, in the first one by H interaction of OH (phenol) with an OH of the catalyst and in the second, by the formation of a phenolate species between an O (OH phenol) and Mn^{n+}.

Keywords Mn–Ce composite · Phenol oxidation · Phenolate · Carboxylate · Monodentate phenoxy group

O. D'alessandro · H. J. Thomas · J. E. Sambeth (✉)
Centro de Investigación y Desarrollo en Ciencias Aplicadas "Dr. Jorge J. Ronco" UNLP CCT CONICET LA PLATA, 47 Nro 257 (1900), La Plata, Argentina
e-mail: sambeth@quimica.unlp.edu.ar

O. D'alessandro · H. J. Thomas · J. E. Sambeth
Fac. Ciencias Exactas UNLP, 47 Y 115 (1900), La Plata, Argentina

H. J. Thomas
Planta Piloto Multipropósito PLAPIMU CICPBA, Gonnet, Argentina

Introduction

Phenol is a chemical product mainly of anthropogenic origin, since in nature it can be found only in the decomposition of organic remains, such as in resins or in wood combustion. The main sources are refineries, petrochemical industries, carbon, pulp and paper, dye and painting, polymer and medical industries [1]. This contaminant has a characteristic smell detected by most people if present in 40 ppb in air, and a few ppm gives taste to water. Its consumption results in health problems, even leading to death [2].

Technologies for decreasing phenol concentration in wastewaters can be classified into separating or destructive methods. The most important separating techniques are distillation by dragging, extraction with organic solvents, adsorption and separation by membranes according to Busca et al. [3]. Among the adsorbents, activated carbon, which has an adsorption capacity ranging from 0.09 to 0.5 g phenol/gC, and polymeric resins are the most widely used. The destructive techniques include humid oxidation with air, catalytic humid oxidation with air, humid oxidation with chemical agents, electrochemical oxidation and photocatalytic oxidation. There is a wide variety of chemical oxidants such as H_2O_2, $KMnO_4$, Cl_2, O_3 and the Fenton reagent (Fe^{2+}/H_2O_2) that are used at industrial level for phenol elimination. In the catalytic oxidation, noble metals (Pt, Pd), transition metal oxides such as Cu, Mn, V, Mo, Ru and polyoxometalates are used. Different supports are used such as Al_2O_3, TiO_2, CeO_2. In general, the working conditions are: (i) pressures above atmospheric pressure (between 0.5 and 20 bar), (ii) temperatures between 100 and 130 °C and (iii) $W_{Catalyst}/W_{phenol}$ ratio between 0.2 and 5 [4–12].

Several researchers have analyzed the phenol oxidation on the study of catalyst performance in terms of elimination and mineralization [13–15]. The intermediate compounds of phenol oxidation have been detected at elevated temperatures and pressure such as catechol, hydroquinone, etc. Arena et al. [9], have studied the CWO of phenol on Mn–Ce–O catalyst and they have proposed that the reaction is produced in five-step adsorption-oxidation: (i) adsorption on the surface, (ii) interaction substrate/sorbent, (iii) Phenolic intermediate species (solid/liquid equilibrium) (iv) the CO_x formation and (v) the reoxidation of the surface,

In this work, the experimental conditions were milder (atmospheric pressure and 100 °C) than reported in the literature [4–12] with a view to analyze the adsorbed species formed in the first step of the phenol adsorption-oxidation on the Mn–Ce catalyst by DRIFTS spectroscopy.

Experimental

Catalyst preparation

The solids were prepared by the co-precipitation technique from aqueous solutions of metallic salts (0.1 M $Ce(NO_3)_3$ and 2 M $Mn(NO_3)_2{\cdot}4H_2O$) in basic medium at room temperature, according to Imamura et al. [11], using 3 M KOH or 3 M NaOH as precipitating agents. The solids were prepared with molar ratios Mn–Ce: 0–100,

50–50 and 100–0. The obtained samples were washed with doubly distilled water until no Na or K cations were detected. Then they were dried at 100 °C and calcined at 350 °C in air for 3 h. The nomenclature used for defining them is Mn–Ce(M) 0–100, 50–50, 100–0 with M = K or Na.

A portion of the samples Mn–Ce(Na), after being dried, were impregnated with a Cu^{2+} salt using wet impregnation method. The solids were dried at 100 °C, calcined at 350 °C for 3 h following the technique described by Tang [12]. The nomenclature used for each solid is Mn–Ce(Na)Cu 0–100, 50–50, 100–0. By means of the atomic absorption technique, Cu (% w/w) concentration was determined, by a simple balance of Cu between initial and final concentration. These values were found: 3.87; 3.88; 3.84 for Mn–Ce(Na)Cu 0–100, 50–50 and 100–0, in order.

Characterization

The solids were analyzed by X-ray diffraction (XRD), in a Philips PW 1390 equipment with CuK_{α} radiation. The XPS study was carried out in a Multitechnique System equipment (SPECS) with a source of dual X-rays of Mg/Al and a hemispheric analyzer PHOIBOS 150 operating in FAT (fixed analyzer transmission) mode. The binding energy (BE) was calculated using C1s = 284.6 eV as internal reference. The bulk composition and C concentration were analyzed by means of EDS (Energy-Dispersive X-ray Spectroscopy). The specific BET surface area was measured in a sorptometer Micromeritics Accussorb 2100D. Temperature programmed reduction (TPR) experiments were performed in a Quantachrome equipment Quantasorb Jr., using 25–50 mg of sample in powder form (previously ground monolith). In all cases, the temperature was increased from ambient to 900 °C at a heating rate of 10 °C min^{-1}. A gas mixture of H_2–N_2, 5 % by volume was used as reducing gas, a total flow rate of 22 ml min^{-1}. Copper oxide was used for the calibration of the equipment.

Catalytic activity

Deionized water was used in the preparation of phenol solutions. The study was carried out at 100 °C in a batch glass reactor (volume = 250 ml), at atmospheric pressure with constant stirring at 2,700 rpm. The reactor is equipped with a condenser, which opens to the atmosphere, to prevent the evaporation of phenol. The initial phenol concentration (Cph_o) was set at 1,000 ppm. The $W_{Catalyst}/W_{phenol}$ ratio was 2. Liquid samples were withdrawn as a function of reaction time (Cph) and were determined by UV–Vis spectroscopy (Perkin-Elmer Lambda 35) at a wavelength of 270 nm corresponding to the second phenol maximum. A calibration curve was used to analyze the remaining concentration of phenol. As all the catalysts have different specific surface areas, two phenol removal are defined;

(a) phenol removal of the solution defined as

$$\left(1 - \frac{\text{Cph}}{\text{Cph}_\text{o}}\right) \times 100 = \text{Phenol Removal}\,(\%)$$

(b) Specific removal (SR), which represents the ratio between phenol removal of solution (%) at 4 h and the specific surface area of each catalyst.

DRIFT spectroscopy

The DRIFTS analysis was carried out in Bruker Vertex 70 equipment using a cell Spectra Tech 0030-011. After the reaction, the samples were dried in N_2 atmosphere at room temperature for 24 h. The DRIFT spectra were obtained in N_2 atmosphere, with a spectral resolution of 4 cm^{-1} and accumulation of 500 scans at RT.

Results and discussion

Characterization

The XRD spectra are shown in Fig. 1a–c. The results show the formation of Mn_2O_3 (JCPDS # 41-1442) and MnO_2 (JCPDS # 81-2261) in the solids Mn–Ce(Na) 100–0 and 50–50. In the solids Mn–Ce(Na) 50–50 and 0–100, the XRD patterns confirm

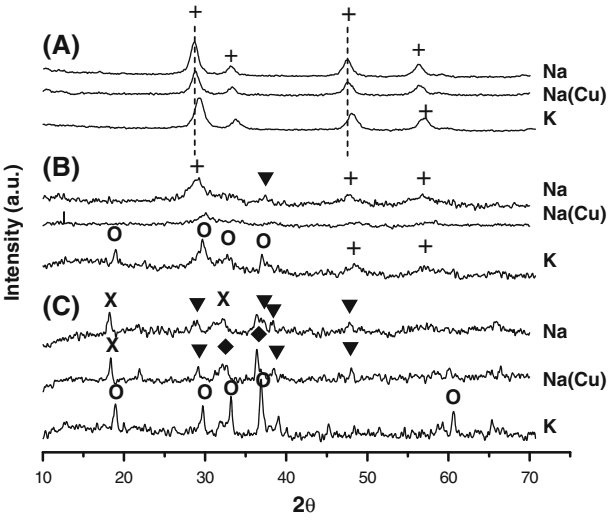

Fig. 1 XRD patterns of Mn–Ce samples; **a** Mn–Ce(M) 0–100; **b** Mn–Ce(M) 50–50 and **c** Mn–Ce(M) 100–0 with M = Na or K. *Symbols*: (**+**) CeO_2; (**O**) Cryptomelane; (**X**) Mn_2O_3; (*black down poiniting triangle*) MnO_2; (*black diamond*) $Cu_{1+X}\ Mn_{2-X}O_4$

the presence of CeO_2 (with fluorite-type structure JCPDS # 43-1002). In the samples Mn–Ce(Na)Cu 100–0, the presence of spinel Cu (JCPDS # 70-0262) is detected. As can be seen the solid Mn–Ce(Na)Cu 50–50 presents poor crystallinity.

In the Mn–Ce(K) 100–0 and Mn–Ce(K) 50–50 samples, the presence of cryptomelane phase (OMS-2 JCPDS 34-168) is detected. As can be observed in Fig. 1a, when K is added to the structure, the diffraction diagram of Mn–Ce(K) 0–100 shows a shift towards a higher θ than those for the solids precipitated with Na and the ones subsequently impregnated with Cu. According to Hussain et al. [13], this phenomenon is due to a strong K-support interaction. The absence of diffraction peaks corresponding to CuOx allows us to suggest that Cu is very well dispersed.

Fig. 2 shows the XPS spectrum of Mn2p for samples 100–0 and 50–50 precipitated with Na and K. In the solids Mn–Ce(Na) 50–50 and (K) 50–50, a shift of 0.8 eV with respect to Mn–Ce(M) 100–0 is observed. According to Larachi et al. [14], this phenomenon is attributed to Mn–Ce interaction. Besides, according to Xing et al. [15], the symmetry observed in the spectrum $Mn2p_{1/2}$ is evidence of the lack of Mn^{2+} species, and this agrees with the Mn crystalline species found by XRD.

As Galakhov et al. [16] point out, the energy levels of orbital 3d of transition metals show a change in the splitting due to the electronic interaction 3s–3d, the splitting magnitude being inversely proportional to the valence state of Mn. Using the method suggested by Oku et al. [17] for the determination of the average oxidation states (AOS) of Mn, the values for each sample were calculated and are listed in Table 1. These results show that Mn has an AOS between 3.57 and 3.69,

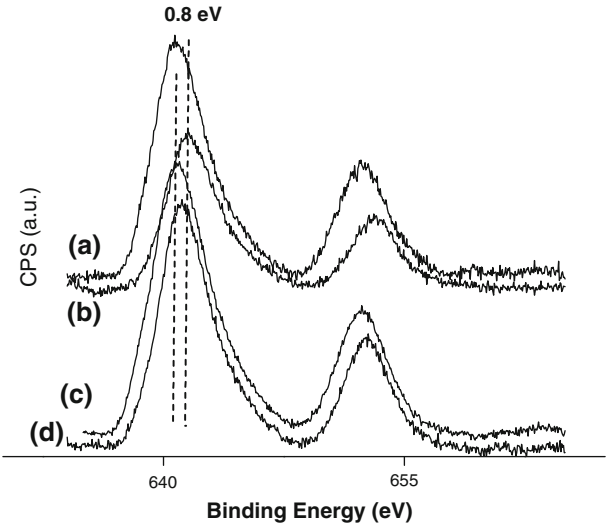

Fig. 2 XPS spectrum of Mn2p for samples 100–0 and 50–50: **a** Mn–Ce(K) 100–0; **b** Mn–Ce(K) 50–50; **c** Mn–Ce(Na) 100–0; **d** Mn–Ce(Na) 50–50

Table 1 Average oxidation states of Mn

Sample	AOS
Mn–Ce(K) 100–0	3.64
Mn–Ce(K) 50–50	3.57
Mn–Ce(Na) 100–0	3.69
Mn–Ce(Na) 50–50	3.63
Mn–Ce(Na)Cu 100–0	3.62
Mn–Ce(Na)Cu 50–50	3.86

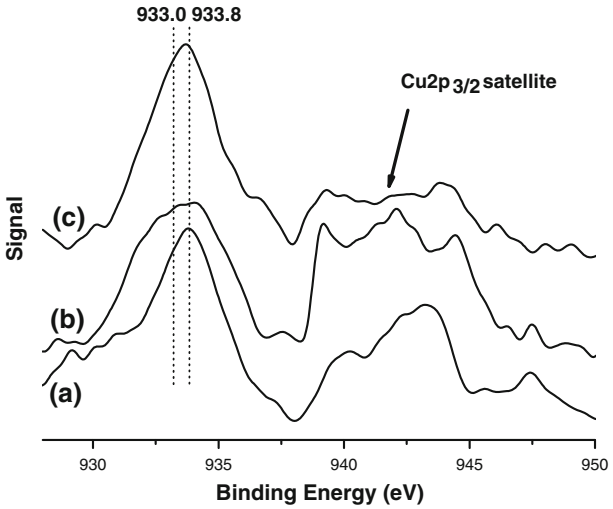

Fig. 3 XPS spectrum of Cu2p: **a** Mn–Ce (Cu) 100–0; **b** Mn–Ce (Cu) 50–50; **c** Mn–Ce (Cu) 0–100

reaching a value higher than 3.80 only in the catalyst Mn–Ce(Na) Cu 50–50. These results are in agreement with Tang et al. [18] who have estimated an AOS between 3.9 and 3.2 in Mn–Ce catalyst by TPR and XPS. As can be seen both XRD and XPS results show the presence of Mn^{3+} and Mn^{4+}.

The XPS spectrum of Cu2p (Fig. 3) presents a signal at 933.0 eV assigned to Cu^{+} and another at 933.8 eV, which is attributed to Cu^{2+}[19].

Fig. 4 shows the XPS spectrum of Ce3d. The dotted lines indicate the valleys between peaks V (882.5 eV) − V′ (888.7 eV) and U (901.0 eV) − U′(906.7 eV), which, according to studies by Ji et al. [20], are directly linked to the amount of Ce^{3+}, the deeper the valley is, the lower the concentration of Ce^{3+}. According to Damynova et al., [21] the U″ peak is characteristic of Ce(IV). If we compare the different solids (Table 2), we can see that the Ce^{4+} concentration in the presence of Na ion is higher than the concentration when KOH is used like the precipitating agent.

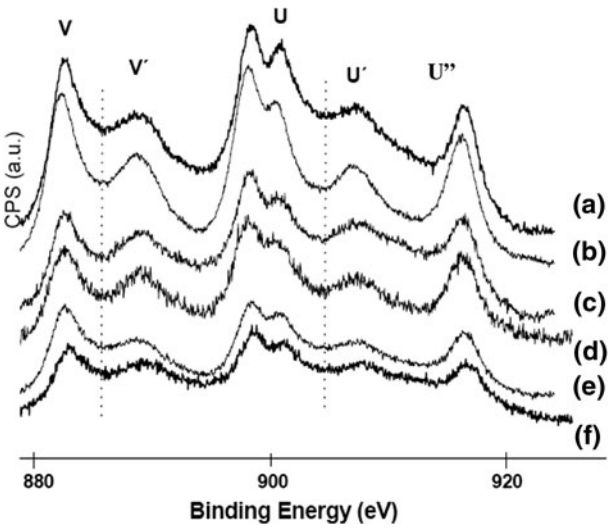

Fig. 4 XPS spectrum of Ce3d: **a** Mn–Ce(K) 50–50; **b** Mn–Ce(K) 0–100; **c** Mn–Ce(Na) 50–50; **d** Mn–Ce(Na) 0–100; **e** Mn–Ce(Na)Cu 50–50; **f** Mn–Ce(Na) Cu 0–100

Table 2 Relative Ce^{4+} proportions in the solids

Sample	Ce^{4+} ratio
Mn–Ce(K) 0–100/Mn–Ce(K)50–50	2.97
Mn–Ce(Na) 0–100/Mn–Ce(Na) 50–50	1.91
Mn–Ce(Na)Cu 0–100/Mn–Ce(Na)Cu 50–50	1.10
Mn–Ce(Na) 50–50/Mn–Ce(K) 50–50	8.21
Mn–Ce(Na) 50–50/Mn–Ce(Na)Cu 50–50	2.60
Mn–Ce(K) 50–50/Mn–Ce(Na)Cu 50–50	0.34
Mn–Ce(Na) 0–100/Mn–Ce(K)0–100	5.00
Mn–Ce(Na) 0–100/Mn–Ce(Na)Cu 0–100	4.45
Mn–Ce(K) 0–100/Mn–Ce(Na)Cu 0–100	0.89

Table 3 XPS O1s data measured

Sample	O_I (%)	O_{II} (%)	O_I-BE (eV)	O_{II}-BE (eV)
Mn–Ce(K) 0–100	52.9	46.1	528.8	530.4
Mn–Ce(K)50–50	72.9	27.1	529.1	531.2
Mn–Ce(K) 100–0	62.9	36.1	528.8	530.8
Mn–Ce(Na) 0–100	58.5	41.5	528.4	530.4
Mn–Ce(Na) 50–50	71.3	28.7	529.0	530.6
Mn–Ce(Na) 100–0	54.7	45.3	528.8	530.4
Mn–Ce(Na)Cu 0–100	50.5	49.5	528.7	530.4
Mn–Ce(Na)Cu 50–50	73.5	21.3	529.5	532.2
Mn–Ce(Na)Cu 100–0	59.5	40.5	528.9	530.8

On the other hand, from the analysis of Figs. 2 and 4, it follows that Mn does not modify the cerium chemical environment since its peaks do not change their position, though the Mn environment is indeed affected by Ce, as is shown by the 0.8 eV shift detected at 50–50 with respect to 100–0.

According to Larachi et al. [14], in this type of compounds, the lattice oxygens (O_I) are found between a BE of 528.9 and 529.7 eV, while the oxygen ions (O_{II}) bonded to metallic cations with low coordination are found between 531.0 and 532.0 eV. The position and concentration of each O type in each prepared solid are included in Table 3. It can also be observed that in the solids whose compositions are 50–50, independently of the precipitating agent cation, there is a shift towards higher BE both in O_I and O_{II}. On the surface of the samples, the O_I percentages are 73 % in Mn–Ce 50–50, whereas in the pure solids (0–100 and 100–0), the concentration of O_I oxygens ranges from 50 to 63 %. These results allow us to infer that the interaction between Mn and Ce favors an increase in the concentration of oxygen with their saturated coordination (O_I).

The results of the EDS analysis on the bulk composition of Mn–Ce 50–50 are included in Table 4. While the solids Mn–Ce(Na) and Mn–Ce(Na)Cu are placed in the range of the expected concentration close to 1, the solid precipitated with KOH has a Mn/Ce ratio equal to 2.17. We believe that this result could be associated with the formation of cryptomelane phase in the solid. In this sense, Abecassis et al. [22], who have prepared a series of solids Mn–Ce–O by different techniques, determined by EDS analysis that Ce ions have poor accessibility to the structure due to the strong bond K–Mn–O.

Table 4 EDS analysis: bulk concentration of Mn–Ce(M) 50–50 samples

Sample	Percentages (%)
Mn–Ce(K) 50–50	68.5 (Mn)–31.5 (Ce)
Mn–Ce(Na) 50–50	47.3 (Mn)–52.7 (Ce)
Mn–Ce(Na)Cu 50–50	54.1 (Mn)–45.9 (Ce)

Table 5 Surface areas of Mn–Ce(M) samples

Sample	S_{BET} (m^2/g)
Mn–Ce(K) 100–0	25
Mn–Ce(K) 50–50	88
Mn–Ce(K) 0–100	123
Mn–Ce(Na) 100–0	22
Mn–Ce(Na) 50–50	87
Mn–Ce(Na) 0–100	137
Mn–Ce(Na)Cu 100–0	29
Mn–Ce(Na)Cu 50–50	88
Mn–Ce(Na)Cu 0–100	138

Data of the solid surface area are listed in Table 5. As can be seen, the surface area is independent of the precipitating cation when the composition is 50–50. If we compare the surface of solids precipitated with KOH to that obtained with NaOH and to that impregnated with Cu in the solids 100–0, a decrease close to 10 % when the cation is Na and a 10 % increase in the case of impregnation with Cu are detected. The variations in the specific surface area of different samples could be attributed to the different phases that are formed. Thus, Rives et al. [23] and Hussain et al. [13] associate this effect with the crystalline structure and with the cation effect that forms it, either Cu or K.

Catalytic activity

The first two-step of the phenol oxidation is the interaction between the catalyst and phenol where the adsorption process occurs. Fig. 5 hows the phenol removal on catalysts. The best performance is observed in the Mn–Ce(Na)Cu 50–50 catalyst. We attribute the greater activity of the sample Mn–Ce(Na)Cu 50–50 to the fact that it does not have a defined crystalline structure, which favors the formation of crystalline defects [24, 25] and the interaction Cu–Mn–Ce–O. Moreover, the other two solids impregnated with Cu have a very different activity. As can be seen in the figure, after 4 h of reaction, phenol removal in Mn–Ce(Na)Cu 100–0 is close to

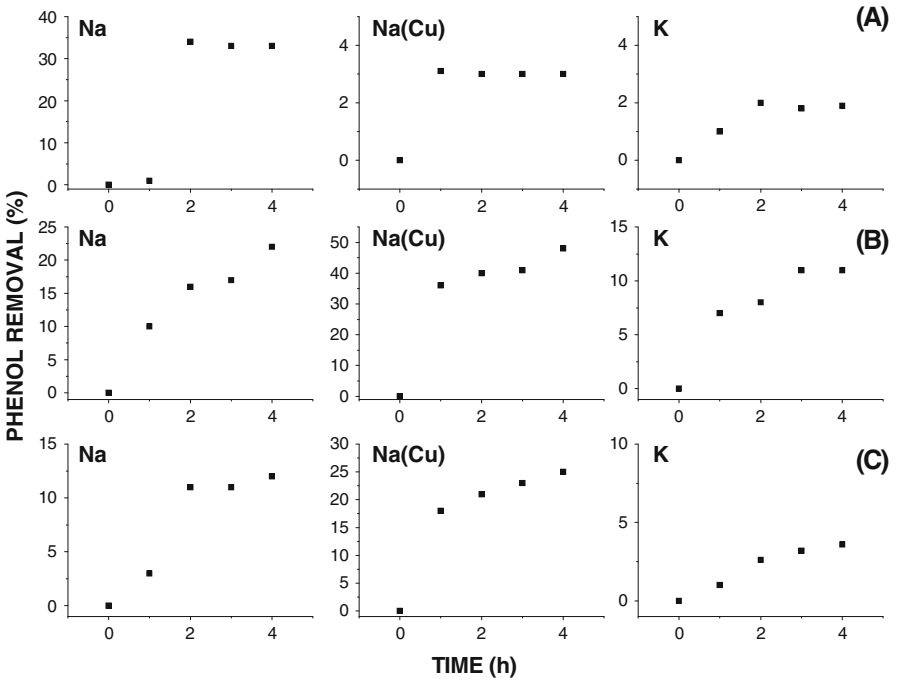

Fig. 5 Phenol removal as a function of the reaction time; **a** Mn–Ce(M) 0–100; **b** Mn–Ce(M) 50–50 and **c** Mn–Ce(M) 100–0 with M = Na or K

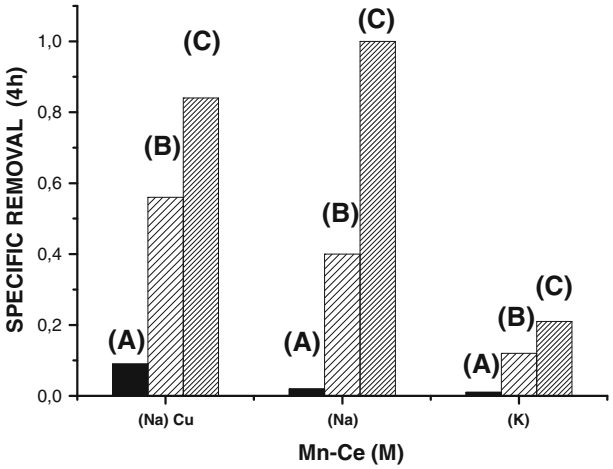

Fig. 6 Phenol specific removal after 4 h of reaction as function of oxide composition. **a** Mn–Ce(M) 0–100; **b** Mn–Ce(M) 50–50; **c** Mn–Ce(M) 100–0

25 %, while the removal in the sample 0–100 is lower than 12 %. These results confirm that the interaction Cu–Ce–O is enhanced by the presence of Mn^{4+} [26].

Fig. 6 shows the phenol specific removal (SR) after 4 h of reaction as a function of each oxide composition. The obtained result suggests that there is a greater dependence on the Mn–Ce–O interaction than on the specific surface area and that Mn is the active species, this phenomenon being in agreement with the results from different authors [7, 9].

From the results, we can also say that the precipitation with NaOH is better for phenol elimination than that with K. According to Cheng and coworkers [27], K in concentrations below 4 % w/w may affect the oxidation state of Mn, resulting in the formation of Mn^{2+} with the subsequent enhancement of the catalytic activity. However, a peak in the zone of 640.4 eV, characteristic of the species Mn^{2+} [28], was not detected by XPS. According to EDS results, K concentration is higher than 6 %, and this is proved by the presence of OMS-2, which is a stable phase. The low catalytic performance as a function of K concentration agrees with what was pointed out by Santiago et al. [29], whose results show that the increase in K load reduces phenol conversion in the Mn–Ce system. Likewise, Cheng et al. [30], who have studied the Mn and K effect on CeO_2 in the hydrogenation of benzoic acid, state that the addition of K causes an increase in the crystal size of CeO_2 strongly affecting the catalytic activity, an effect that can be observed by XRD as above-mentioned.

As it can be seen (Fig. 6), an important Mn influence is observed the solid activity as mentioned above. If we compare the relationship between the structure and the SR the results demonstrated that: (i) in the Mn–Ce(K) solids, the presence of Ce is not as favorable as the formation of cryptomelane structure (Mn–Ce(K) 100–0) in the adsorption of phenol, (ii) in Mn–Ce(Na) samples, the couple Mn^{3+}/Mn^{4+} is the active species in the process and (iii) when Cu is present in the

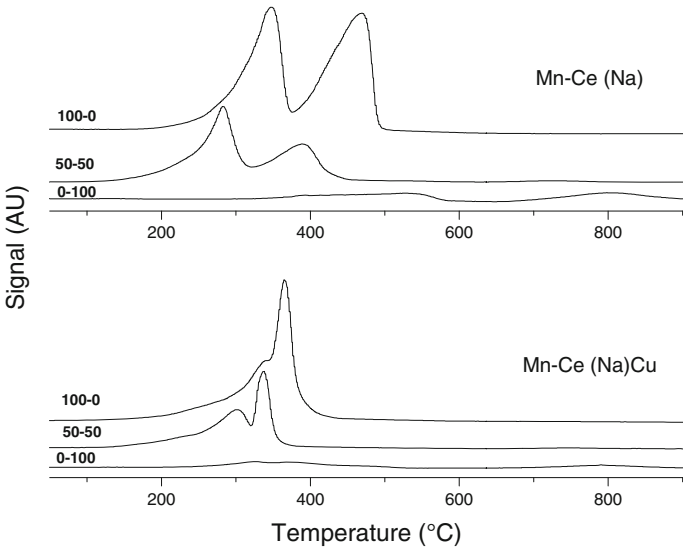

Fig. 7 TPR data obtained for fresh Mn–Ce(Na) and Mn–Ce(Na) Cu solids

Table 6 Carbon elemental analysis of used Mn–Ce(Na) and Mn–Ce(Na)Cu catalysts

Sample	Carbon concentration (% w/w)
Mn–Ce(Na) 0–100	7.5
Mn–Ce(Na) 50–50	11.2
Mn–Ce(Na) 100–0	5.2
Mn–Ce(Na)Cu 0–100	6.4
Mn–Ce(Na)Cu 50–50	13.0
Mn–Ce(Na)Cu 100–0	6. 7

solid solution, the formation of Cu spinel improves the adsorption. H_2-TPR curves of Mn–Ce(Na) and Mn–Ce(Na)Cu are presented in Fig. 7. The TPR results demonstrate that the oxidation states of Mn are modified but both results to say that the presence of Cu in the solids only is favorable when CeO_2 is formed. These results demonstrate the positive effect that Cu has on the system favoring, on the one hand, the transfer processes of Ce^{4+} load [27].

Table 6 lists the weight/weight concentration of C obtained by EDS analysis after the reaction in solids of the series Mn–Ce(Na) and Mn–Ce(Na)Cu. The results show that in sample Mn–Ce(Na)Cu 50–50, the C quantity is higher than in the others, followed by Mn–Ce(Na) 50–50, which has a poor performance. In this regard, the solids with a higher amount of C are those that have a higher concentration of O_I-type oxygens and, according to Tang [18], a surface rich in these species has a high removal of phenol. Fig. 5 shows that phenol removal as a function of the reaction time of each solid is not significant when compared to that reported by different

authors [13, 18]. This phenomenon is attributed to the fact that experimental conditions are moderated and then is impossible to re-oxidize the surface and to oxidize the phenol adsorbed. In this sense, the deactivation of the Mn–Ce catalysts has been studied by several authors who have shown that it is due to the presence of strongly adsorbed carbonaceous species [10, 13, 22, 31]. Besides, reaction intermediates have not been found in the solution, though other authors have detected their presence [32–34] when working with O_2 pressures between 0.5 and 20 bar and temperatures ranging from 100 to 170 °C. In addition, the solubility of oxygen under the experimental conditions of this work is low. The failure to detect intermediates may be due to the reaction conditions without an atmosphere rich in O_2, which may not enable re-oxidizing the surface and favoring the formation of less harmful reaction products.

The analysis between Table 6 and Fig. 6 shows that the content of carbon in the samples after the test is in the range of 6–13 % and taking into account that the initial weight ratio $W_{Catalyst}/W_{phenol}$ is 2, this corresponds to 12–26 % of initial PhOH being present in the catalyst after 4 h of reaction. These results infer that a considerable fraction of phenol has being adsorbed on the surface. As can be seen in Fig. 6, the phenol removal does not increase with the reaction time, which is in accordance with adsorption process. In this sense, Hu et al. [12] have shown that the phenol binding reactions are fast at elevated temperature.

From the obtained results, we can say that the best performance is related to three factors: (i) the concentration of O_I-type oxygen species [35], (ii) a higher concentration of Mn^{4+} [29, 36, 37] and (iii) the redox couple Mn^{3+}/Mn^{4+} seems to provide the active sites for the reaction.

DRIFTS study

Arena et al. [9] have proposed that the adsorption-oxidation of phenol occurs in five steps:

$$PhOH + \alpha \leftrightarrow PhOH(s) \text{ (step i)}$$
$$PhOH(s) + \sigma\text{-}O \rightarrow P(s) + \sigma \text{ (step ii)}$$
$$P(s) \leftrightarrow P(l) \text{ (step iii)}$$
$$P(s) + n\ (\sigma\text{-}O) \rightarrow CO_x \text{ (step iv)}$$
$$\sigma + O_2 \rightarrow \sigma\text{-}O \text{ (step v)}$$

The results have shown that under these experimental conditions, the phenol molecule is adsorbed on the surface, which can be associated with the steps (i) and (ii).

Fig. 8 shows the DRIFTS spectra of Mn–Ce(Na) sample after 4 h of reaction time. In order to improve the observations, the corresponding catalyst was subtracted from each spectrum of adsorbed phenol. Table 7 gives the band assignment. The results demonstrated that the phenol molecule is adsorbed on the solids as a phenolate group and phenol and the relative amount are important in both Mn–Ce(Na) 100–0 and 50–50 solids. According to Mariey et al. [38], in the 1,650–1,200 cm^{-1} range, the bands indicate the presence of an aromatic group (1,633 and 1,494 cm^{-1}) and phenoxy species (1,265 cm^{-1}). The bands at 1,633 and

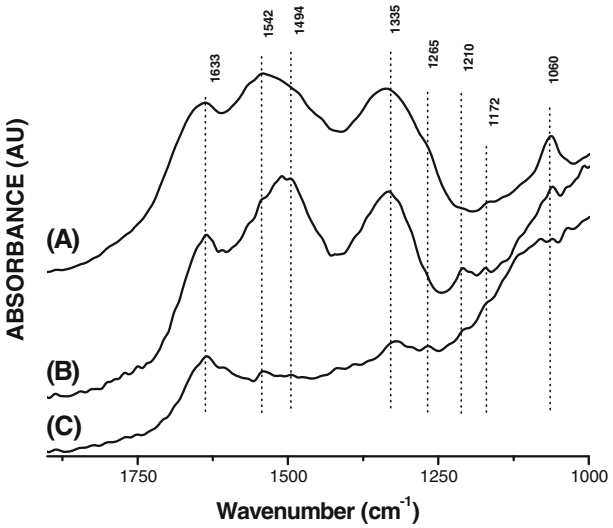

Fig. 8 Spectra of phenol adsorbed species formed on Mn–Ce(Na): **a** 100–0; **b** 50–50; **c** 0–100. Assignation in Table 7

Table 7 Frequencies of DRIFTS peaks from the phenol adsorption-reaction

Frequency (cm^{-1})	Assignment
1,633	C = C ring—aromatic group
1,542	Ring vibration carboxylate species
1,494	νC=C
1,335	δ (OH) plane Carboxylate species
1,265	Monodentade phenoxy
1,210	ν (C–O)
1,172	O–H deformation ν C–O (phenol)
1,060	Phenolate group

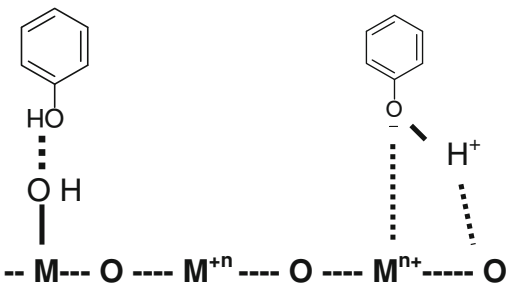

Fig. 9 A possible mechanism of the first stages of adsorption-oxidation of phenol over Mn–Ce catalyst (see text)

1,494 cm^{-1} are assigned to the aromatic group. In particular, the latter band is 10 cm^{-1} lower than the wavenumber of phenol in the gas phase. This result suggested the presence of the interaction phenol-catalyst. On the other hand, the band at 1,265 cm^{-1} is attributed to the formation of monodentate phenoxy group [38]. Finally, the bands at 1,335 and 1,172 cm^{-1} are assigned to OH vibrations and carboxylate groups [39].

According to the DRIFTS results and the theoretical studies of alcohol oxidation on transition metal oxides [40–42], it is suggested that two possible mechanisms of phenol adsorption from an OH group of its molecule may be: (a) chemisorptions through H from a phenol OH group to an OH species of the solid, (b) through the hydrogen of phenol OH species interacting with an O_I close to a cation leading to the formation of a superficial OH and enabling the interaction of O of a phenoxide or phenolate group with an M^{n+} species as seen in Fig. 9. Both species could transform into a phenoxy radical that is responsible for the formation of catechol or hydroquinone as the first intermediate compound according to the mechanism proposed for the complete oxidation of phenol to CO_2 [9, 43]. Finally, these results suggest that the phenol molecule is adsorbed in the first step as phenolate and Mn^{4+} could be the active site in the process.

Conclusions

Mn–Ce samples were prepared by alkaline co-precipitation using NaOH and KOH as precipitating agents. A part of those obtained with Na were dried and impregnated with a Cu^{2+} salt. The characterization results allow determining that different cations influence not only the formation of the crystalline phase but also the distribution of Mn/Ce in the bulk and surface phases, and the Ce oxidation state. The solids were evaluated in the phenol removal at 100 °C and at atmospheric pressure, with the aim to analyze the adsorbed species in the first steps in the oxidation reaction.

The results determine that Mn cations are the active species and that K concentration is an important factor in the activity of solids due to its influence on the solid structure. The interaction Mn–Ce-Cu is favorable to the process. The best performance is related to the concentration of O_I-type oxygen species and the higher Mn^{4+} concentrations.

The DRIFTS results suggested that phenol is adsorbed by two mechanisms, first by H of an OH group of phenol interacting with a superficial hydroxyl and second, through the formation of a phenolate species on a Mn site.

Acknowledgments The authors are grateful to CONICET, UNLP and ANPCYT of Argentina for financial support.

References

1. Jordan W, van Barnevel H, Gerlich O, Kleine M, Ulrico J (2002) "Ullmann's encyclopaedia of industrial" chemistry. Wiley-VCH Verlag, New York

2. Canadian Environmental Protection Act, Priority Substances List Assessment Report: Phenol (2000) Minister of Public Works and Government Services
3. Busca G, Berardinelli S, Resini C, Arrighi L (2008) J Hazard Mater 160:265–288
4. Sanabria N, Molina R, Moreno S (2010) Catal Lett 130:664–671
5. Resini C, Catania F, Berardinelli S, Paladino O, Busca G (2008) Appl Catal B 84:678–683
6. Zhar S, Wang X, Huo M (2010) Appl Catal B 97:127–134
7. Hu B, Chen C, Frueh S, Jin L, Joesten R, Suib S (2010) J Phys Chem 114:9835–9844
8. Abecassis-Wolfovich M, Landau M, Brenner A, Herskowitz M (2004) Ind Eng Chem Res 43:5089–5097
9. Arena F, Negro J, Parmaliana A, Spadaro L, Trunfio G (2007) Ind Eng Chem Res 46:6724–6731
10. Kouraichi R, Delgado J, López Castro J, Stitou M, Rodriguez Izquierdo J, Cauqui M (2010) Catal Today 154:195–201
11. Imamura S, Dol A, Ishida S (1985) Ind Eng Chem Prod Res Dev 24:75–80
12. Tang X, Chen J, Li Y, Li Y, Xu Y, Shen W (2006) Chem Eng J 118:119–125
13. Hussain S, Sayari A, Larachi F (2001) Appl Catal B 34:1–9
14. Larachi F, Pierre J, Adnot A, Bernis A (2002) Appl Surf Sci 195:236–250
15. Xing X, Yu P, Xu M, Wu X, Li S (2008) J Phys Chem C 112:15526–15531
16. Galakhov V, Demeter M, Bartkowski S, Neumann M, Ovechkina N, Kurmaev E, Lobachevskaya N, Ya M, Mukovskii J, Mitchell J, Ederer D (2002) Phys Rev B 65:113102–113106
17. Oku M (1995) J Elec Spectrosc Relat Phenom 74:135–148
18. Tang X, Li Y, Huang X, Xu Y, Zhu H, Wang J, Shen W (2006) Appl Catal B 62:265–273
19. Chapelle A, Yaacob M, Pasquet I, Presmanes L, Bernabé A, Tailhades P, Du Pleiss J, Kalantarzadeh K (2011) Sens Actuators B: Chem 153:117–124
20. Ji P, Zhang J, Chen F, Anpo M (2008) J Phys Chem C 112:17809–17813
21. Damynova S, Bueno J (2003) Appl Catal A 253:135–141
22. Abecassis-Wolfovich M, Jothiramalingam R, Landau M, Herskowitz M, Viswanathan B, Varadarajan T (2005) Appl Catal B 59:91–98
23. Rives V, Del Arco M, Prieto M (2004) Bol Soc Esp Ceram V 43:142–147
24. Peluso M, Sambeth J, Thomas H (2003) React Kinect Catal Lett 80:41–47
25. Li T, Chiang S, Liaw B, Chen Y (2011) Appl Catal B 103:143–148
26. Li J, Zhu P, Zhou R (2011) J Power Sour 196:9590–9598
27. Cheng D, Hou Ch, Chen F, Zhan X (2009) React Kinet Catal Lett 97:217–223
28. Magne P, Walker P (1986) Carbon 24:101–107
29. Santiago A, Sousa J, Guedes R, Jerônimo C, Benachour M (2006) J Hazard Mater 138:325–330
30. Cheng D, Hou Ch, Chen F, Zhan X (2009) J Rare Earths 27:723–727
31. Arena F, Italian C, Ranieri A, Saja C (2010) Appl Catal B 99:321–328
32. Bride M, Kung K (1991) Environ Toxicol Chem 10:441–448
33. Bhargava S, Tardio J, Prasad J, Folger K, Akolekar D, Grocott S (2006) Ind Eng Chem Res 45:1221–1258
34. Hamoudi S, Sayari A, Belkacemi K, Bonneviot L, Larachi F (2000) Catal Today 62:379–388
35. Zhang H, Yang W, Li D, Wang X (2009) React Kinect Catal Lett 97:263–268
36. Picasso G, Gutiérrez M, Pina M, Herguido J (2007) Chem Eng J 126:119–130
37. Shi L, Chu W, Qu F, Luo S (2007) Catal Lett 113:59–64
38. Mariey L, Lamotte J, Lavalley J, Tsyganenko N, Tsyganenko A (1996) Catal Lett 41:209–211
39. Abbas O, Rebufa C, Dupuy N, Kister J (2008) Talanta 77:200–209
40. Tang X, Chen J, Li Y, Li Y, Xu Y, Shen W (2006) Chem Eng J 118:119–125
41. Lamaita L, Peluso M, Thomas H, Sambeth J, Minelli G, Porta P (2005) Catal Today 107–108:133–138
42. Sambeth J, Juan A, Gambaro L, Thomas H (1997) J Mol Catal A: Chem 118:283–291
43. Andrade L, Laurindo E, de Oliveira R, Rocha-Filho R, Cass Q (2006) J Braz Chem Soc 17:369–373